re-BUS

You have downloaded a document from
RE-BUŚ
repository of the University of Silesia in Katowice

Title: Pionic fusion in light-ion systems

Author: L. Joulaeizadeh, I. Gasparić, H.R. Amir-Ahmadi, J. Bacelar, R. Caplar, M. Eslami-Kalantari, Elżbieta Stephan i in.

Citation style: Joulaeizadeh L., Gasparić I., Amir-Ahmadi H.R., Bacelar J., Caplar R., Eslami-Kalantari M., Stephan Elżbieta i in. (2011). Pionic fusion in light-ion systems. "Physics Letters B" (Vol. 694, iss. 4-5 (2011), s. 310-315), doi 10.1016/j.physletb.2010.10.015

Uznanie autorstwa - Licencja ta pozwala na kopiowanie, zmienianie, rozprowadzanie, przedstawianie i wykonywanie utworu jedynie pod warunkiem oznaczenia autorstwa.

UNIWERSYTET ŚLĄSKI W KATOWICACH
Biblioteka Uniwersytetu Śląskiego
Ministerstwo Nauki i Szkolnictwa Wyższego

Physics Letters B 694 (2011) 310–315

Contents lists available at ScienceDirect

Physics Letters B

www.elsevier.com/locate/physletb

Pionic fusion in light-ion systems

L. Joulaeizadeh [a,*], I. Gašparić [b], H.R. Amir-Ahmadi [a,1], J. Bacelar [a], R. Čaplar [b], M. Eslami-Kalantari [a,2], N. Kalantar-Nayestanaki [a], H. Löhner [a], H. Mardanpour [a], J.G. Messchendorp [a], H. Moeini [a], A. Ramazani-Moghaddam-Arani [a], S.V. Shende [a], E. Stephan [c]

[a] KVI, University of Groningen, Groningen, The Netherlands
[b] Rudjer Bošković Institute, Zagreb, Croatia
[c] Institute of Physics, University of Silesia, Katowice, Poland

ARTICLE INFO

Article history:
Received 9 April 2010
Received in revised form 1 September 2010
Accepted 8 October 2010
Available online 14 October 2010
Editor: V. Metag

Keywords:
Pionic fusion
Neutral pion production
Subthreshold energy
Clustering correlation

ABSTRACT

The role of pions in the nuclear interaction has been studied in pionic fusion experiments using the AGOR accelerator facility at KVI. Pionic fusion is a highly coherent process in which two nuclei fuse to a united nucleus and the available centre-of-mass (C.M.) energy is emitted through the pion channel. The examined reactions were ^{4}He(^{3}He,π^0)^{7}Be and ^{6}Li(^{4}He,π^0)^{10}B* and both reactions were performed at C.M. energies about 10 MeV above the coherent pion production threshold. Here, the experimental results for the ^{6}Li(^{4}He,π^0)^{10}B* reaction will be presented and discussed. In order to provide sensitivity to the full dynamics and relevant processes involved in the pionic fusion reaction, almost the full angular distribution of neutral pions has been determined. In a phenomenological analysis, the contributions of Legendre polynomials to reproduce the behaviour of the angular distribution have been studied. The results of this analysis confirm the importance of the clustering correlations for the ^{6}Li(^{4}He,π^0)^{10}B* reaction. The mass dependence of the pionic fusion reaction is in agreement with the results of the existing models extrapolated to this reaction.

© 2010 Elsevier B.V. All rights reserved.

1. Introduction

The pion plays a significant role in modelling the nuclear forces and explaining the structure of the nucleus. In collisions between two free nucleons, pions can be produced if the C.M. energy of the nucleon–nucleon (NN) system exceeds the pion mass m_π. In addition to pion production in the free NN interaction, pions have been produced in nuclear reactions at collision energies per nucleon which are considerably below the threshold energy in the free NN system [1–13]. In the extreme limit of the pion production, called pionic fusion, the total excess energy is concentrated in the pion field, the pion is emitted and the colliding nuclei fuse to form a united nucleus (fusion product) in a specific bound state

$$A_1 + A_2 \rightarrow \pi + B(J, I). \tag{1}$$

$B(J, I)$ denotes the (bound) united nucleus with spin and isospin quantum numbers J and I, respectively. Obviously the two reaction products have to carry away the total free energy. The C.M. kinetic energy T_{CM} in the incident channel is transferred to the two-body exit channel including the pion field: $T_{CM} = T^{ex}_{CM} + Q_{A_1,A_2,B} + m_\pi c^2$, where T^{ex}_{CM} and Q denote the available energy above the coherent threshold in the C.M. system and the energy released in the complete fusion process without pion emission, respectively. Pionic fusion reactions open up kinematical properties of collective behaviour which are not accessible in free NN collisions. Since the production of a single pion demands a significant fraction of the available energy, a highly coherent mechanism is required. The angular distribution of the pionic fusion cross sections may provide the full dynamic information on the pion production and the pion re-scattering. Therefore, the differential cross sections provide sensitivity to the relevant multipolarities involved in the pion production process.

The complete microscopic calculation of the pionic fusion process is a theoretical challenge. There are some theoretical models [14–17] aiming to describe the scarce available experimental data and all models are in favour of clustering phenomena [16] since the required high relative energy among colliding nucleons might originate from many-body correlations. Due to the low cross section (in the order of nb), pionic fusion experiments are not easily performed. The reported experimental data, mainly in light sys-

* Corresponding author.
E-mail address: l.joulaeizadeh@tudelft.nl (L. Joulaeizadeh).
[1] Present address: Department of Physics, Faculty of Science, University of Kashan, Kashan, Iran.
[2] Present address: Department of Physics, Yazd University, Yazd, Iran.

0370-2693/$ – see front matter © 2010 Elsevier B.V. All rights reserved.
doi:10.1016/j.physletb.2010.10.015

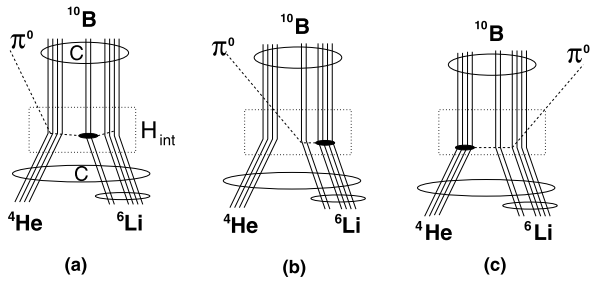

Fig. 1. Schematic representation of the possible reaction mechanisms for the ^{6}Li(^{4}He, π^0)^{10}B* reaction, taking the strong clustering correlations into account. The dashed square represents the pion production operator "H$_{int}$" and "C" denotes the clustering correlations.

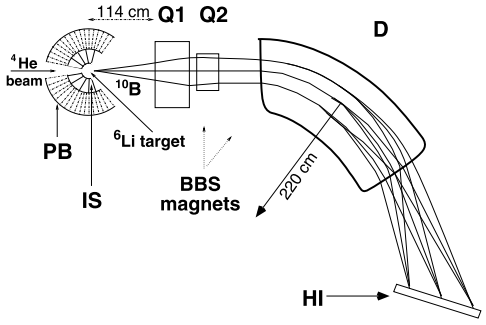

Fig. 2. A cross section view of the experimental setup showing the PB together with its IS, the BBS including its magnets (Q1, Q2 and D) and the HI detector.

tems, mostly provide the total cross section of charged pion production, and rarely complete angular distributions were measured. The latest reported results of the pionic fusion experiments correspond to the total cross sections of the ^{12}C(^{12}C, ^{24}Mg)π^0 [8], ^{12}C(^{12}C, ^{24}Na)π^+ [8] and ^{2}H(^{4}He, ^{6}Li*)π^0 [2,3] reactions where only the fusion products have been measured. In a model restricting the pion–nucleon interaction to the single-nucleon Born term [17], the measured cross section of 208 ± 38 pb for the ^{12}C(^{12}C, ^{24}Mg)π^0 reaction is underestimated by a factor of 10! The cause of this discrepancy is difficult to understand since the existing data do not clearly separate the structure of the final state. Furthermore, the aim of the ^{2}H(^{4}He, ^{6}Li*)π^0 experiment was to use the pionic fusion of a deuteron and an alpha particle as a probe particularly sensitive to the cluster structure of the isobaric analogue state of the ground state of ^{6}He, at 3.56 MeV excitation energy in ^{6}Li.

This situation calls for the new differential cross section data for pionic fusion reaction, collected in measurements which are selective in choice of the final state and cover almost the full angular range. Two pionic fusion experiments have been performed and investigated at KVI using the AGOR facility. The ^{4}He(^{3}He, π^0)^{7}Be experiment used a 0.3 nA ^{3}He beam on a 140 mg/cm^2 liquid ^{4}He target [18]. In the ^{6}Li(^{4}He, π^0)^{10}B* experiment, a 3 nA ^{4}He beam on a 2 mg/cm^2 ^{6}Li target was used [19]. Both experiments were carried out at only 10 MeV above the coherent threshold in the C.M. system. Here we focus the discussion of the experimental results on the ^{6}Li(^{4}He, π^0)^{10}B* reaction, while the detailed analysis of the ^{4}He(^{3}He, π^0)^{7}Be experiment will be the subject of forthcoming publications [18,20]. We identified the reaction cross section by measuring the fused system and the produced π^0 with large acceptance. According to the available energy above the threshold (10 MeV) and the isospin conservation, only a few excited states in ^{10}B are allowed. Since many of these states decay by the emission of particles which are not fully accepted in the applied experimental setup, only the ^{10}B states at E = 1.7402 MeV ($J^P = 0^+$, $I = 1$) and partly at E = 5.1639 MeV ($J^P = 2^+$, $I = 1$) could contribute to the cross section measured in our experiment. The latter excited state contributes with 85% according to the ratio of gamma and particle decay widths.

Considering the possible cluster configurations, the pionic fusion processes for the ^{6}Li(^{4}He, π^0)^{10}B* reaction may schematically be drawn as shown in Fig. 1. In the first process the pion is emitted from the deuteron which is transformed into a "quasi deuteron" with $I = 1$ and $J = 0$ as has been suggested for the modelling of the ^{2}H(^{4}He, ^{6}Li*)π^0 reaction [2]. The pion is then re-scattered on one (or both) of the alpha particles which retains its identity (Fig. 1(a)). In the second and third process the pion is emitted from one of the alpha particles which either belongs to the target or the projectile and then is re-scattered by the other alpha particle and (or) the "quasi deuteron" (Fig. 1(b) and (c)). Subsequently the "quasi deuteron" and the two alpha particles form ^{10}B*.

The main goal of the present work is to measure the angular distribution of the pionic fusion cross section in order to study systematically the effect of clustering and the influence of increased complexity in the clustered systems. In addition, the total cross sections of the examined reactions have been measured and compared with the predicted results of two different existing models [16,17] for the mass dependence of the pionic fusion cross section. The present experimental setup provided the angular distribution of the cross section by measuring all the reaction products in over-determined kinematics. Only in this way one can guarantee clean and truly exclusive data. Furthermore, in the examined reactions with well-defined initial and final state configurations, simple clustered systems are involved which demand less complicated theoretical work to model the reaction.

2. Experimental setup

For the detection of low-momentum neutral pions, a highly segmented 4π detector system, the Plastic Ball detector (PB) [21], was used. The PB consists of phoswich modules built from a 4 mm CaF_2 crystal and a 356 mm plastic scintillator. The plastic scintillator acts as a light-guide for the thin CaF_2 crystal. In the present configuration, the PB covers 77% of 4π solid angle and polar angles between 50° and 160°. Since neutral pions decay with a mean life time of $(8.4 \pm 0.6) \cdot 10^{-17}$ s still in the target to two photons with a probability of 98.8%, the PB was used to detect two photons. In order to improve the detector response and efficiency for photons, the hollow sphere in the centre of the PB is equipped with another segmented 2π-detector system, the Inner Shell detector (IS) [24], consisting of 5 cm thick CsI(Tl) scintillators. For the detection and identification of ions with $4 \leqslant Z \leqslant 6$ and typical energies of 10–43 AMeV, a specially designed array of phoswich scintillators in a segmented layer, the Heavy Ion detector (HI) [23], was employed. Each of the phoswich modules has a cuboid geometry consisting of a 4 cm × 1.3 cm × 1.3 cm CsI(Tl) crystal and a 80 μm thin plastic scintillator covering one 4 cm × 1.3 cm face of the CsI(Tl) crystal. The momentum resolution of ions detected by individual modules of the HI array corresponds to the horizontal position resolution. In commissioning experiments [23], a momentum dispersion of 0.6% per detector unit was determined. This calibration results in a binning of 0.6% in the ion momentum spectrum. The HI array was placed in the vacuum chamber in front of the nominal focal plane of the Big–Bite Spectrometer (BBS) [22]. The BBS is a QQD-type magnetic spectrometer which was positioned near 0° to deflect and momentum analyse fusion products emitted at small scattering angles.

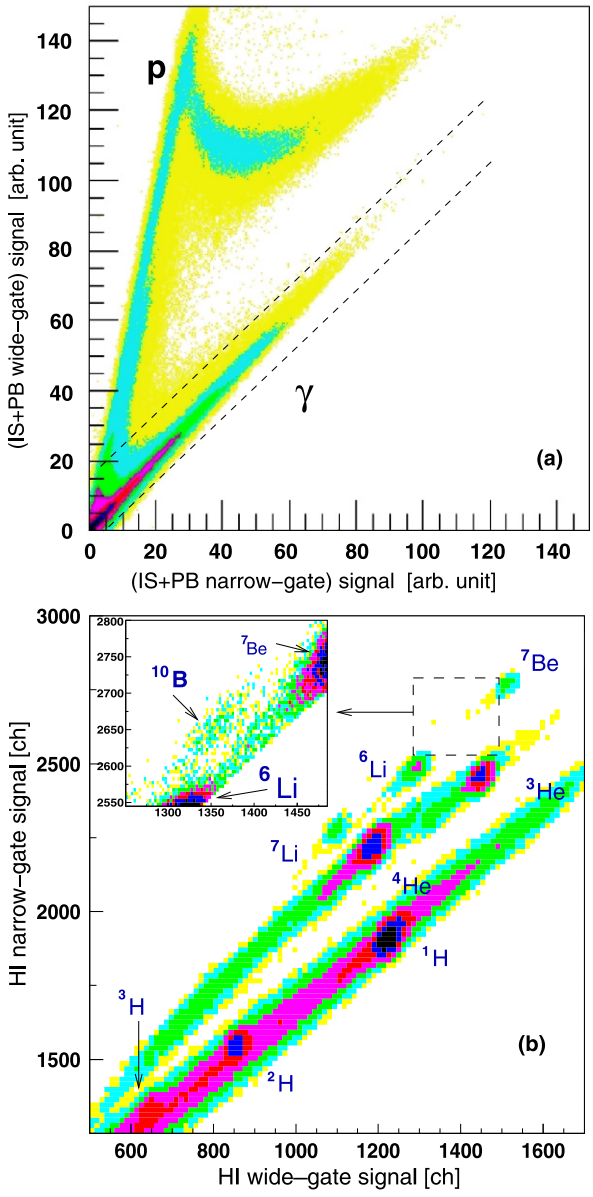

Fig. 3. (a): The PB plus IS pulse shape and identification of photons. The spectrum is summed over all modules. Regions labelled "p" and "γ" represent events associated with protons and photons, respectively. The horizontal (vertical) axis shows the sum of the IS and the plastic (the IS, CaF_2 and the plastic) light output. The intensity scale is logarithmic. (b): The HI pulse shape and identification of ions. The horizontal (vertical) axis represents the total (plastic) light output, in one HI detector module. The light output is given in units of channels of the digitiser which amplified the plastic component by a factor of 5. The intensity scale is logarithmic. The region of the ^{10}B peak summed over all the HI detector modules is shown enlarged in the insert.

A cross section view of the employed experimental setup is shown in Fig. 2.

3. Results

Fig. 3(a) shows the identification of photons by the two-dimensional spectrum (pulse shape spectrum) produced using the wide- and narrow-gate integration of the signal for the PB detector module. To calibrate the PB and IS detector modules, the measured signal from high energy cosmic muons was exploited [24]. The calibrated results are confirmed by the results of the Monte Carlo simulation using the detector simulation package GEANT3 [25]. The charged particles which are mainly protons, are well separated from the photon line. A two-dimensional spectrum produced using the wide- and narrow-gate integration of the signal for a single HI detector module in coincidence with two photons in the PB is shown in Fig. 3(b). The peaks indicate the produced ions with different energies in the ^{4}He + ^{6}Li reaction. Using Time Of Flight (TOF) from the target to the HI detector, the produced ions have been identified [19]. However, ions with the same m/q ratio (e.g. ^{4}He, ^{6}Li and ^{10}B) have the same TOF. Therefore, other available information was required to obtain a unique identification of ^{10}B. The results of the calibration experiments done by Horn et al. [26,27] were used as a tool to obtain the pure plastic and the pure CsI(Tl) light output of the HI detector [19,23] taking strong quenching effects into account. The relative light output of the HI detector for the produced ions is in agreement with the results of the Horn measurements at equivalent ion energies. In order to achieve the required accuracy in particle identification in the region of the ^{10}B peak, the calibration of all HI detector modules was based on the well-determined positions of the ^{6}Li and ^{7}Be ions in the pulse-shape spectrum. A detailed analysis of the HI detector light output, including the possible saturation effects caused by the photomultipliers will be reported [18].

Examining the events in the PB which were registered every time a ^{10}B nucleus was identified in the BBS, we have seen a clear enhancement of two-photon occurrences. Since in the ^{6}Li(^{4}He,π^0)^{10}B* experiment the available energy above the coherent threshold was 10 MeV, the produced pions have small kinetic energy. Therefore, the observed two photons are primarily emitted with large opening angles ($\theta_{\gamma\gamma}$) as expected for the two-photon decay of π^0's, moving with small velocity in the laboratory. In Fig. 4(a), the solid histogram shows the measured opening-angle distribution of two photons by measuring the positions of PB detector modules hit by two photons. The dashed histogram corresponds to the result of the phase-space simulation. The measured opening-angle distribution covers the same region as the result of the phase-space simulation with a peak at around 147°. The identification of neutral pions is based on the invariant mass analysis of the detected two-photon events. The observables needed for the identification of π^0 through the invariant mass analysis are the energy of two photons from π^0 decay (E_{γ_1} and E_{γ_2}) and the opening angle $\theta_{\gamma\gamma}$ between them:

$$M_{\gamma\gamma} = \sqrt{2E_{\gamma_1}E_{\gamma_2}\left(1-\cos(\theta_{\gamma\gamma})\right)}. \quad (2)$$

Since low-energy photons are detected with worse energy resolution due to threshold effects in neighbouring detector modules, only the energy of the photon with the higher energy deposition was taken from the photon measurement. This value together with the measured ^{10}B momentum in the HI detector and the total available energy in the experiment were used to obtain the energy of the photon with the lower energy deposition. Fig. 4(b) shows the two-photon invariant mass distribution. The solid and dashed histograms are the results of the measurement and the phase–space simulation, respectively. The widths of the invariant mass distributions are the result of the experimental angular and energy resolutions. The sharp cut at about 150 MeV is caused by the kinematical limits imposed by the energy conservation. Compared to the simulated invariant mass distribution the experimental one appears broader and shifted by up to 5 MeV to lower mass values. However, both distributions are compatible within the uncertainty in the peak positions (sqrt(variance) of the weighted mean) of both distributions which is about 3.5 MeV. In order to check how a possible shift in the experimental invariant mass by up to 4% with respect to the simulation would affect the detector acceptance, we studied the GEANT3 simulation for an arbitrarily shifted invariant

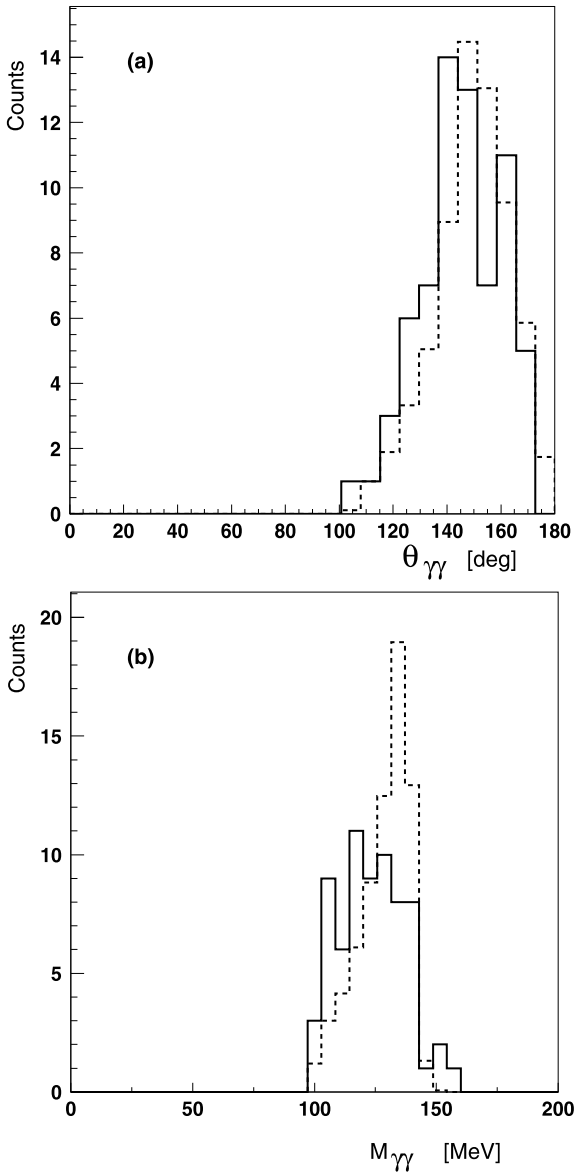

Fig. 4. (a): The solid histogram shows the measured opening-angle distribution of two photons from the PB detector. The dashed histogram shows the opening-angle distribution of two photons from the phase-space simulation of the ^{6}Li(^{4}He, π^0)^{10}B* reaction. (b): The two-photon invariant mass distribution from the measurement (the solid histogram) and the phase-space simulation (the dashed histogram, scaled to the yield of the measured distribution).

mass by modifying the high-energy photon by 8%. The maximum expected change in the acceptance is about 6%, mostly at backward angles.

4. Differential cross sections

Fig. 5(a) shows the differential cross sections as a function of pion polar angle in the C.M. system integrated over the pion full azimuthal angle range. Full circles are the results of the ^{6}Li(^{4}He, π^0)^{10}B* measurement at KVI at the incident energy of $T_{beam}/nucleon = 59.1$ MeV. For comparison, the triangles represent the data from the ORSAY experiment [5] for the ^{4}He(^{3}He, π^+)^{7}Li reaction at the incident energy of $T_{beam}/nucleon = 88.8$ MeV. The curves represent the results of the theoretical predictions based on Ref. [16]. The thin black curve is the result obtained using the cluster model wave function of ^{7}Be in the ^{4}He(^{3}He, π^0)^{7}Be reaction at $T_{beam}/nucleon = 88.8$ MeV. The thick grey and black curves are the results calculated with the use of, respectively, the cluster model and the shell model wave functions of ^{7}Li from the ^{4}He(^{3}He, π^+)^{7}Li reaction at $T_{beam}/nucleon = 88.8$ MeV. A local imaginary potential W_D, which attenuates with the incident wave in the entrance channel, has been adopted in the calculations. All the solid curves were obtained when $W_D = -25$ MeV, while the dashed curves are the results when $W_D = 0$ MeV. Up to now, there is no theoretical calculation available for the ^{6}Li(^{4}He, π^0)^{10}B* reaction. Calculations for the other reactions are shown to guide the eye and to give an indication how and where the results should be expected. Only the statistical uncertainties of the measured results are displayed in Fig. 5(a). The systematic error includes uncertainties in the measurement of the beam current (8%), the live time of the data acquisition electronics (12%), and the determination of the detector acceptances (2%), summing up to ±15%.

5. Analysis and discussion

For a phenomenological analysis of the angular distributions, the following expression for the differential cross section has been assumed:

$$\left(\frac{d\sigma}{d\Omega}\right)_{c.m.} = \sum_{n=0}^{i} a_n P_n\left(\cos\theta_{c.m.}^{\pi^0}\right), \tag{3}$$

where $P_n(\cos\theta_{c.m.}^{\pi^0})$ are the Legendre polynomials and $\theta_{c.m.}^{\pi^0}$ is the C.M. angle of π^0. We call a_n the Legendre coefficients. Eq. (3) was fitted to the results of the clustering model for the ^{4}He(^{3}He, π^0)^{7}Be reaction (the thin black curve in Fig. 5(a)) as well as the ^{6}Li(^{4}He, π^0)^{10}B* experimental results. The aim was to study which different contributions of the Legendre polynomials are responsible to reproduce the asymmetric behaviour of the angular distribution and produce the same shape of the differential cross section as the prediction of the cluster model. Furthermore, it would be interesting to explore which component of the Legendre polynomial expansion plays the most important role. By comparing the fitted results of the ^{4}He(^{3}He, π^0)^{7}Be calculation and the ^{6}Li(^{4}He, π^0)^{10}B* measurement, one may get insight whether the assumption of strong clustering correlations also holds for the ^{6}Li(^{4}He, π^0)^{10}B* reaction. There are no pions measured at $\theta_{c.m.}^{\pi^0} < 40°$ and $\theta_{c.m.}^{\pi^0} > 150°$. Thus another aim of fitting was to extrapolate the polynomial fit to cover the full angular range in order to calculate the total cross section of the ^{6}Li(^{4}He, π^0)^{10}B* reaction.

It is concluded that the fit up to the third polynomial order ($i = 3$) from Eq. (3) is the lowest order polynomial fit to the clustering calculation with a high confidence level (see Table 1). By fitting Legendre polynomials from Eq. (3) to the ^{6}Li(^{4}He, π^0)^{10}B* experimental results, it was noted that the polynomial fit with $i = 3$ follows the same trend as the fit with $i = 3$ to the ^{4}He(^{3}He, π^0)^{7}Be calculation. The quality of this fit to the ^{6}Li(^{4}He, π^0)^{10}B* results is as good as that to the calculated results of the ^{4}He(^{3}He, π^0)^{7}Be reaction. We conclude that the fit with $i = 3$ is the lowest order fit to describe the ^{6}Li(^{4}He, π^0)^{10}B* experimental results. In Fig. 5(b), the final accepted Legendre polynomial fits with $i = 3$ are shown. The thin black curve shows the results of the cluster model for the ^{4}He(^{3}He, π^0)^{7}Be reaction. The dashed curve is the fitted curve to the ^{4}He(^{3}He, π^0)^{7}Be results of the cluster model. The data points are the ^{6}Li(^{4}He, π^0)^{10}B* experimental results and the dotted curve is the fitted curve to the ^{6}Li(^{4}He, π^0)^{10}B* measured results. The Legendre coefficients (a_n) as well as the χ^2 of the fits are listed in Table 1. The variance in the fit parameters a_n is the square root of the diagonal entry in the covariance matrix. In case of the ^{4}He(^{3}He, π^0)^{7}Be reaction, the contribution of $P_2(\cos\theta_{c.m.}^{\pi^0})$ is the

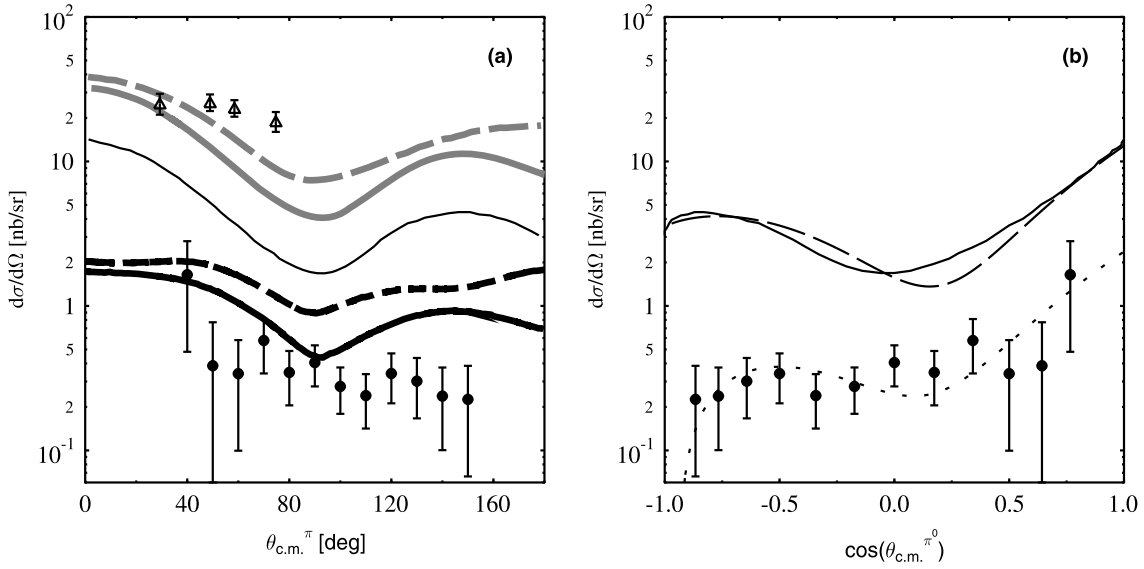

Fig. 5. Angular distribution of pionic fusion reaction cross section at subthreshold energies. (a): Full circles are the results of the KVI experiment for the ^{6}Li(^{4}He,π^0)^{10}B* reaction. Triangles are the results from the ORSAY experiment for the ^{4}He(^{3}He,π^+)^{7}Li reaction. The thin black curve is the result of the cluster model for the ^{4}He(^{3}He,π^0)^{7}Be reaction. The thick grey and black curves are the results based on, respectively, the cluster and shell model for the ^{4}He(^{3}He,π^+)^{7}Li reaction. All the solid and dashed curves were obtained when $W_D = -25$ and 0 MeV, respectively. (b): The same as (a) for thin black curve and full circles. The dashed curve is the result of the polynomial fit to the ^{4}He(^{3}He,π^0)^{7}Be calculated results of the cluster model. The dotted curve is the result of a polynomial fit to the ^{6}Li(^{4}He,π^0)^{10}B* experimental data.

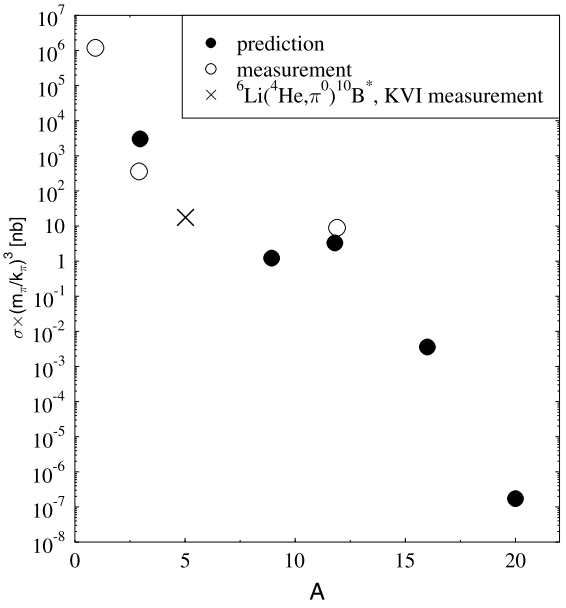

Fig. 6. The general behaviour of the pionic fusion cross section $A+A \rightarrow \pi+2A(J,I)$ versus the average of projectile and target mass. k_π and m_π are the pion momentum and mass, respectively. The full circles are the calculated results from the model described in Ref. [17]. The empty circles are the measured results of the previous experiments [8,4]. The cross is the result of the KVI measurement for the ^{6}Li(^{4}He,π^0)^{10}B* reaction.

largest to reproduce the theoretical results, while to reproduce the ^{6}Li(^{4}He,π^0)^{10}B* experimental results, the $P_1(\cos\theta^{\pi^0}_{c.m.})$ contribution is the largest. However, still the $P_2(\cos\theta^{\pi^0}_{c.m.})$ and $P_1(\cos\theta^{\pi^0}_{c.m.})$ contributions are comparable.

From Fig. 5(b), it should be noted that the measured angular distribution is anisotropic. The shape of the measured differential cross sections of the ^{6}Li(^{4}He,π^0)^{10}B* reaction is as predicted for the ^{4}He(^{3}He,π^0)^{7}Be reaction (the thin black curve) by taking strong clustering correlations into account [16]. Due to the asymmetric target-projectile combination in the ^{6}Li(^{4}He,π^0)^{10}B* reaction, the angular distribution of the cross section is forward–backward asymmetric. According to the Microscopic reaction model developed by L. Harzheim et al. [15], the angle of the minimum in the angular distribution depends on how much target and projectile contribute to the pion production process. The symmetric ^{3}He(^{3}He,π^+)^{6}Li reaction should exhibit an angular distribution which is symmetric around $\theta^{\pi^+}_{c.m.} = 90°$. However, in case of a dominant target contribution the conclusion of this model for the ^{3}He(^{3}He,π^+)^{6}Li reaction is that the minimum of the angular distribution is found at $\theta^{\pi^+}_{c.m.} < 90°$. Applying this argument to the result of the polynomial fit to the ^{6}Li(^{4}He,π^0)^{10}B* experimental data (Fig. 5(b) dotted curve) in which the minimum is found at $\theta^{\pi^0}_{c.m.} < 90°$, π^0 in the ^{6}Li(^{4}He,π^0)^{10}B* reaction should dominantly be emitted from the ^{6}Li target side. Furthermore, due to the isospin conservation rules and the available C.M. energy, the differential cross section of the ^{6}Li(^{4}He,π^0)^{10}B* reaction should be exhausted by the type (a) of the reaction mechanism shown in Fig. 1. It is consistent with the explanation of the target emission. Therefore, the π^0 angular distribution is expected to be mainly backward peaked since in the entrance channel the deuteron moves to the backward direction. However, based on the extrapolation of the polynomial fit to the forward angles of the ^{6}Li(^{4}He,π^0)^{10}B* angular distribution (the dotted curve in Fig. 5(b)), the measured differential cross section of the ^{6}Li(^{4}He,π^0)^{10}B* reaction is forward peaked. One possible explanation could be that still the second and the third reaction mechanisms contribute and effectively change the angular distributions from the backward to a forward peaked distribution.

By integrating the fitted curve, the total cross section for the ^{6}Li(^{4}He,π^0)^{10}B* reaction was obtained (see Table 1). It should be noted that the calculated total cross section of 47.4 nb for the ^{4}He(^{3}He,π^0)^{7}Be reaction from the polynomial fit is in good agreement with 47.3 nb from the cluster model. The total cross section of the neutral pion production for the ^{6}Li(^{4}He,π^0)^{10}B* reaction follows the same trend as was predicted by the model discussed in Ref. [17]. The result is shown in Fig. 6 by the cross. Using the polynomial fit, the extrapolated cross section of the ^{6}Li(^{4}He,π^0)^{10}B* reaction at $\theta^{\pi^0}_{c.m.} = 0°$ is 2.4 nb/sr and is lower than the pre-

Table 1
Legendre coefficients, the χ^2 of the fits and the total cross sections obtained from the fitting of Eq. (3) to the results of the ^{6}Li(^{4}He,π^0)^{10}B* experiment and to the results of the cluster model for the ^{4}He(^{3}He,π^0)^{7}Be reaction. The uncertainties are purely statistical. "CC" and "PFCC" indicate "Cluster Calculation" and "Polynomial Fit to Cluster Calculation", respectively.

Reaction T_{beam} [MeV]	a_0 [nb/sr]	a_1 [nb/sr]	a_2 [nb/sr]	a_3 [nb/sr]	a_1/a_0	a_2/a_0	a_3/a_0	χ^2	σ_{tot} [nb]
^{6}Li(^{4}He,π^0)^{10}B*									
$T_{beam} = 236.4$ KVI	0.54	0.68	0.59	0.57	1.26	1.09	1.06	1.07	6.8
measurement	±0.09	±0.32	±0.88	±0.15	±0.63	±1.64	±0.33		±0.7
^{4}He(^{3}He,π^0)^{7}Be	3.78	1.77	4.42	2.87	0.47	1.17	0.76	0.65	47.4
$T_{beam} = 266.4$, PFCC	±0.38	±1.11	±0.27	±0.32	±0.30	±0.14	±0.11		
^{4}He(^{3}He,π^0)^{7}Be									47.3
$T_{beam} = 266.4$, CC									

dicted value for the ^{4}He(^{3}He,π^+)^{7}Li reaction. This confirms the decreasing trend of the cross section with increasing mass, which has been predicted by the cluster model [16]. This model predicts values of 11.4 and 2.3 nb/sr for the ^{4}He(^{3}He,π^+)^{7}Li and the ^{16}O(^{3}He,π^+)^{19}F reactions, respectively. In addition, the ratios of the Legendre coefficients are presented in Table 1. A significant asymmetry (a_1/a_0) of the angular distribution is observed in both data sets.

6. Summary

Differential cross sections of the ^{6}Li(^{4}He,π^0)^{10}B* reaction, with well-defined initial and final state configurations, have been presented and discussed. For the first time the almost full pion angular distribution from a pionic fusion reaction with a projectile heavier than ^{1}H has been measured. The experiment was carried out at only about 10 MeV above the coherent threshold energy of pion production in the C.M. system. We identified the reaction by measuring the fused system and the produced π^0 with large acceptance. The total cross section of 6.8 nb was determined for this reaction. The rather specialised theoretical work to completely explain the pionic fusion reaction of ^{6}Li(^{4}He,π^0)^{10}B* still needs to be performed. According to the results of this work, there are hints of strong clustering correlations in the entrance and exit channels of the ^{6}Li(^{4}He,π^0)^{10}B* reaction. It was found that in case of the ^{6}Li(^{4}He,π^0)^{10}B* reaction, the total pionic fusion cross section is in agreement with the extrapolated results of the model discussed in Ref. [17].

Acknowledgements

We thank AGOR accelerator staff for providing high quality beam and GSI for support and the loan of the Plastic Ball. The support of P. Dendooven and H. Timersma in operating the LHe target is gratefully acknowledged. This work was performed as part of the research program of the Stichting voor Fundamenteel Onderzoek der Materie (FOM) with financial support from the Nederlandse Organisatie voor Wetenschappelijk Onderzoek (NWO).

References

[1] J. Eggermann, et al., Z. Phys. A 273 (1975) 384.
[2] M. Andersson, et al., Phys. Lett. B 481 (2000) 165.
[3] M. Andersson, et al., Nucl. Phys. A 779 (2006) 47.
[4] Y. Le Bornec, et al., Phys. Rev. Lett. 47 (1981) 1870.
[5] L. Bimbot, et al., Phys. Lett. B 114 (1982) 311.
[6] L. Bimbot, et al., Phys. Rev. C 30 (1984) 739.
[7] N. Willis, et al., Phys. Lett. B 136 (1984) 334.
[8] D. Horn, et al., Phys. Rev. Lett. 77 (1996) 2408.
[9] E. Aslanides, et al., Phys. Lett. B 108 (1982) 91.
[10] T.E. Ward, et al., Phys. Rev. C 36 (1987) 2680.
[11] C. Richard-Serre, et al., Nucl. Phys. B 20 (1970) 412.
[12] E. Rossle, R.D. Bent, AIP Conf. Proc. 79 (1981) 171.
[13] M.G. Huber, K. Klingenbeck, R. Hupke, Nucl. Phys. A 396 (1983) 191.
[14] J.F. Germond, C. Wilkin, Phys. Lett. B 106 (1981) 449.
[15] L. Harzheim, M. Huber, B.C. Metsch, Z. Phys. A 340 (1991) 399.
[16] T. Kajino, H. Toki, K. Kubo, Phys. Rev. C 35 (1987) 1370.
[17] A. Volya, S. Pratt, V. Zelevinsky, Phys. Rev. C 59 (1999) 305.
[18] I. Gašparić, Ph.D. thesis, University of Zagreb, in press.
[19] L. Joulaeizadeh, Ph.D. thesis, University of Groningen, ISBN: 978-90-367-3804-0 (printed version), 978-90-367-3803-3 (digital version).
[20] I. Gašparić, et al., in press.
[21] A. Baden, et al., Nucl. Instrum. Methods 203 (1982) 189.
[22] A.N. van den Berg, Nucl. Instrum. Methods B 99 (1995) 637.
[23] I. Gašparić, et al., Nucl. Instr. Meth. A, submitted for publication.
[24] L. Joulaeizadeh, et al., Nucl. Instrum. Methods A 204 (2010), doi:10.1016/j.nima.2010.06.
[25] R. Brun, et al., GEANT3 User's Guide, Data Handling Division DD/EE/84-1, CERN, (1986).
[26] D. Horn, et al., Nucl. Instrum. Methods A 320 (1992) 273.
[27] D. Fox, et al., Nucl. Instrum. Methods A 374 (1996) 63.